

A Novel Dioxythiophene Based Conducting Polymer as Electrode Material for Supercapacitor Application

Mehmet Giray Ersozoglu¹, Hans-Detlev Gilsing², Asli Gencturk³ and A. Sezai Sarac^{1,3*}

¹ Polymer Science and Technology, Istanbul Technical University, Istanbul 34469, Turkey

² Institute of Thin Film and Microsensoric Technology (IDM), Kantstr. 55, 14513 Teltow, Germany

³ Nanoscience and Nanoengineering, Istanbul Technical University, Istanbul 34469, Turkey

*E-mail: sarac@itu.edu.tr

Received: 5 July 2019 / Accepted: 6 August 2019 / Published: 30 August 2019

The electrochemical polymerization of the functionalized 3,4-propylenedioxythiophene derivative ProDOT-EtO-BZA **1** bearing an oligoether spacer with aromatic carboxylic group was achieved on platinum (Pt) wire and screen printed carbon electrode (SPCE), respectively. The structure, morphology and electrochemical properties of the PProDOT-EtO-BZA films were analyzed by FT-IR, SEM, AFM and electrochemical impedance spectroscopy (EIS), respectively. Furthermore, poly(3,4-propylenedioxythiophene) (PProDOT), the 2,2-dibenzyl derivative (PDBProDOT) and the 2,2-diethyl derivative (PProDOT-Et₂) were electrodeposited onto SPCE via cyclic voltammetry (CV) for comparison of the capacitance performance of these PProDOTs in organic electrolytes to the corresponding data of PProDOT-EtO-BZA. CV and EIS measurements of the PProDOT-EtO-BZA revealed pseudo-capacitive behavior with faradaic reactions. Specific and low frequency capacitance (20.8 mF/cm² and 8.5 mF/cm², respectively) of the PProDOT-EtO-BZA were almost two times higher than those of the other PProDOTs. These results suggest that PProDOT-EtO-BZA films can be utilized as electrode material for supercapacitors.

Keywords: ProDOT, Supercapacitor, Electrochemical Impedance Spectroscopy, Equivalent-Circuit Model, Screen Printed Electrode.

1. INTRODUCTION

Electrically conductive polymers (CPs) have gained increasing attention due to their unique physicochemical properties exploited in various types of devices and applications like electrochromic displays [1], solar cells [2], supercapacitors [3,4], tissue engineering [5], fuel cells [6], ion-selective electrodes [7] and biosensors [8].

Recently, supercapacitors which are characterized by high power density, long term stability and fast charge/discharge capability has become a remarkable alternative and complementary device to

lithium based conventional batteries [9]. In fact, supercapacitors for different sectors have been successfully commercialized (i.e. power management, consumer electronics, health industry, and transportation) [10–14]. CPs were firstly utilized in supercapacitors in the middle of the 1990s [15] and there is much evidence that these materials operate most efficiently as electrodes for asymmetric supercapacitors [16]. Among the CPs, polythiophene derivatives were widely investigated for supercapacitor application [17]. However, n-doped polythiophene exhibits low stability against oxygen and moisture and is further characterized by its lower conductivity compared to the p-doped polymer [18]. In order to cope with easy oxidation and short cycle life in devices the band-gap has been reduced by introduction of phenyl, methyl and alkoxy substituents in 3-position of the thiophene ring [19-21].

Poly(3,4-alkylenedioxythiophene)s show several advantages over conventional polythiophenes like low oxidation potential, good conductivity, reversibility of optical switching between oxidized and reduced state and high environmental stability [22]. Due to blocking of the 3- and 4- position of the thiophene ring no α - β and β - β coupling during the electropolymerization occurs, so that structurally ordered polymers of high conjugation lengths were obtained. 3,4-Dioxythiophene based polymers were elaborated in order to stabilize the oxidized state and for ensuring solubility and processability of the polymeric material [23].

In this communication, we report on the electropolymerization of the monomeric oligoether carboxyl functionalized ProDOT derivative **1** on platinum wire and SPCE and the investigation of its supercapacitor behavior compared to other PProDOTs electrochemically deposited onto SPCE.

2. EXPERIMENTAL

2.1. Materials

3,4-Propylenedioxythiophene (ProDOT) and 3,4-(2',2'-diethylpropylene)dioxythiophene (ProDOT-Et₂) were obtained from Sigma-Aldrich and used as received. 3,4-(2',2'-Dibenzylpropylenedioxy)thiophene (DBProDOT) and ProDOT-EtO-BZA **1** (Figure 1) were synthesized at the Institute of Thin Film and Microsensoric Technology (IDM), Teltow, Germany according to published procedures [24,25]. Acetonitrile (ACN) (Merck) and tetrabutylammonium hexafluorophosphate (Bu₄NPF₆) (Sigma-Aldrich) were used without further purification. SPCEs were purchased from DropSens. The working electrode in SPCEs had a diameter of 0.4 cm resulting in a geometric area of 0.126 cm² and a calculated area of 0.109 cm² [26].

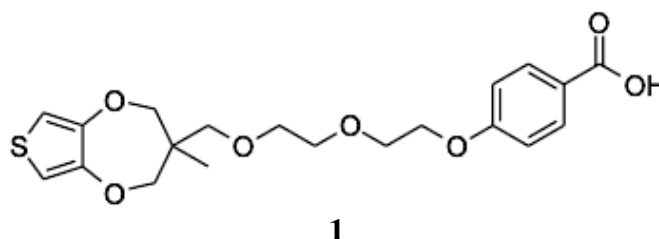


Figure 1. Molecular structure of ProDOT-EtO-BZA **1**

2.2. Polymerization and Characterization

Electropolymerizations were performed by CV using a Princeton Research Potentiostat (model 2263) potentiostat/galvanostat interfaced to a computer with Power Suite software package. The potentiostat was also connected to a Faraday cage (BASi C3 Cell Stand). Syntheses of polymer films were performed by CV on SPCE and Pt wire electrode at ambient conditions. Pt wire of 0.8 cm length was dipped into ~5 ml of electrolyte using a standard three electrode cell (the working electrode had a surface area of 0.171 cm²). Platinum and silver wire electrodes were used as counter and pseudo reference electrodes, respectively and each was placed at a distance of ~1 cm from the other.

SPCE consisted of the carbon working electrode, the carbon counter electrode, and the silver paste reference electrode.

The modified working electrodes were removed from the cell and then washed thoroughly with ACN to remove traces of the monomer. The electrodes were characterized in monomer-free solution to investigate the redox behavior at different scan rates between 20 mVs⁻¹ and 250 mVs⁻¹ by CV.

EIS measurements were conducted at room temperature in the same monomer-free electrolyte using a conventional three electrode cell configuration in monomer-free electrolyte in a frequency range between 10 MHz and 100 kHz with an AC signal amplitude of 10 mV. The electrochemical cell was combined with a potentiostat (PAR 2263) connected to a PC. The EIS data of the system were analyzed using different equivalent circuit models (ECM) and evaluated with the help of ZSimpWin (version 3.30) software from Princeton Applied Research.

3. RESULTS AND DISCUSSION

3.1. Electropolymerization of ProDOT-EtO-BZA on Platinum and SPCE at Different Scan Rates

Electrodepositions were carried out in order to determine the optimum conditions in 0.1 M Bu₄NPF₆/ACN at scan rates of 20, 50 and 100 mVs⁻¹ for 10 cycles using 5 mM ProDOT-EtO-BZA **1** as monomer concentration for deposition onto Pt and SPCE, respectively.

Figure 2 shows the electropolymerization of ProDOT-EtO-BZA **1** at a scan rate of 20 mVs⁻¹ in 0.1 M Bu₄NPF₆/ACN onto Pt wire and SCPE, respectively as the working electrode by CV. The linear increase in current density values for anodic and cathodic peak indicates the formation of the electroactive film on the Pt electrode with each cycle. After washing of the coated working electrode with ACN the redox behavior was investigated in 0.1 M Bu₄NPF₆/ACN by CV. The insets of Figure 2 present the CVs of PProDOT-EtO-BZA films in monomer-free solution at different scan rates. CV curves of the electropolymerization illustrate a regular growth and exhibit a linear increase in current and reversible, well-defined oxidation and reduction peaks as well.

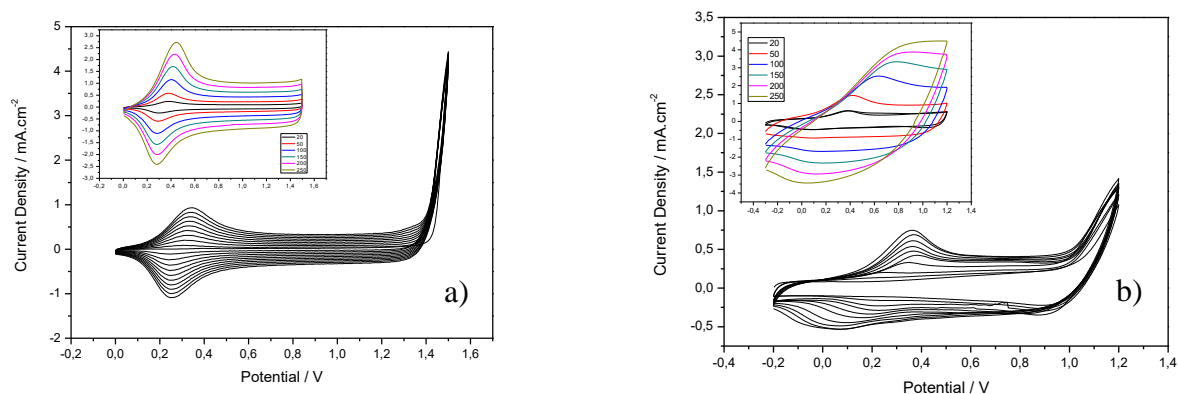


Figure 2. Cyclic voltammograms of the electrogrowth of 5 mM ProDOT-EtO-BZA 1 in 0.1 M $\text{Bu}_4\text{NPF}_6/\text{ACN}$ at 20 mVs^{-1} , 10 cycles. Insets: CV of monomer-free PProDOT-EtO-BZA film in 0.1 M $\text{Bu}_4\text{NPF}_6/\text{ACN}$ at different scan rates between 20 and 250 mVs^{-1} on a) Pt, b) SPCE

During polymer growth, cathodic shifting rate of the reduction peak potential with increasing scan number is more significant on SPCE than on platinum wire electrode what seems to be associated with the formation of a long polymer chain on the SPCE surface due to the chemical structure of the monomer [3].

Monomer-free CV studies of the PProDOT-EtO-BZA on SPCE revealed that the shape of the curves represents pseudocapacitance behavior with faradaic reactions on the electrode surface [27]. In addition, direct proportionality between scan rate (monomer-free) and voltammetry current of the CV and inverse proportionality between capacitance and scan rate (monomer-free) can be interpreted as indicators of an ideally capacitive behavior [28,29].

On the other hand, the platinum electrode coated with polymer film illustrates behavior typical for supercapattery [30] devices at monomer-free CV measurements.

Figure 5 shows the scan rate dependency on current density, for oxidation and reduction peaks of the polymer film coated on SPCE and Pt wire, respectively current density was plotted against the scan rate.

The scan rate dependency of the anodic and cathodic peak currents illustrates a linear relationship to the scan rate and to the square root of the scan rate. As evidenced by the linearity of the plot, R-squared values are approximately 1, this result demonstrates that the electrochemical processes were diffusion-controlled and entirely reversible even at high scan rates [31].

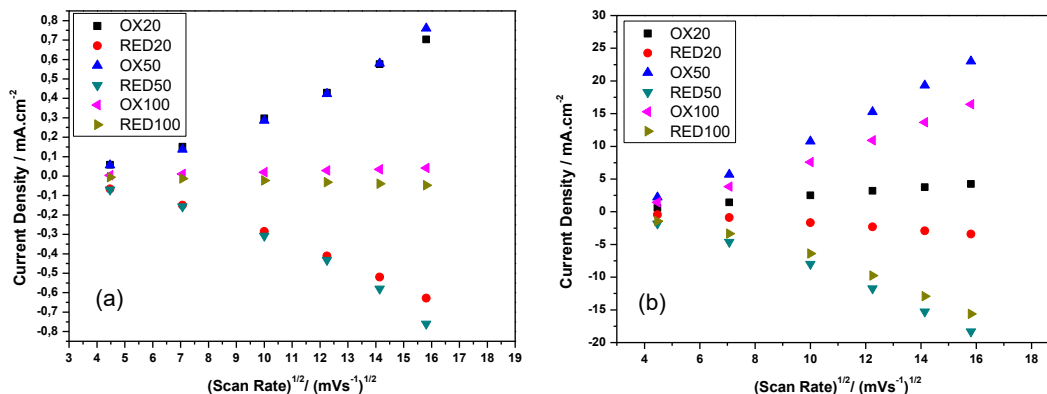


Figure 3. Plots of anodic and cathodic peak current density vs. square root of scan rates for the polymer films in monomer-free solution (in 0.1M Bu₄NPF₆/ACN) of a) Pt wire and b) SPCE.

3.2. EIS investigation and electrical ECM of PProDOT-EtO-BZA

The Nyquist plot of polymer coated Pt wire and SPCE respectively presents a curve typical of a capacitor, without a semi-circle at high frequency region which indicates low interfacial resistances in the system. However, polymer coated Pt wire exhibits a 45° slope at high frequencies with distorted shape associated with semi-infinite diffusion and vertical rise at low frequency indicating an ideal capacitor [32] when electrodeposited at 20 mVs⁻¹ scan rate (Figure 3).

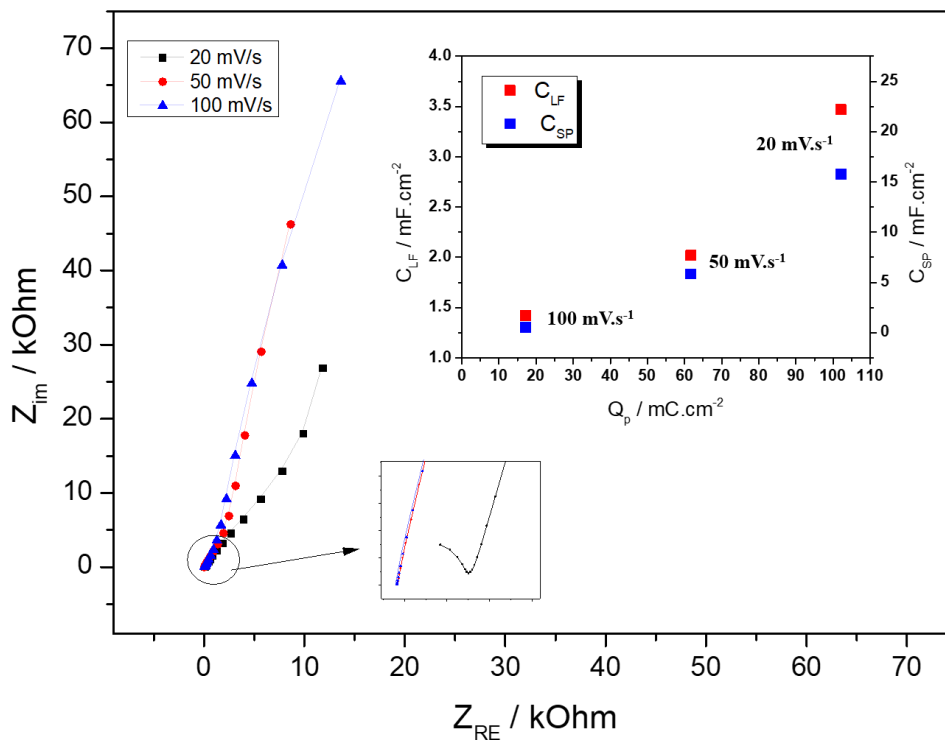


Figure 4. Nyquist plot of PProDOT-EtO-BZA coated at different scan rates on Pt wire in the presence of 0.1M Bu₄NPF₆/ACN, Insets: C_{LF} and C_{SP} (in monomer-free solution, for 20 mVs⁻¹) as a function of polymerization charge (Q_p) of coated films with different scan rates.

The low frequency capacitance (C_{LF}) values from impedance spectroscopy were obtained from the slope of a plot of the imaginary component (Z_{IM}) of the impedance at low frequencies versus the inverse of the reciprocal frequency (f) where ($f = 0.01$ Hz) using eq. (1) [33]

$$C_{LF} = (2\pi \cdot f \cdot Z_{IM})^{-1} \quad (1)$$

PProDOT-EtO-BZA films coated at different scan rates on SPCE showed dominance of the capacitive line, close to 90° , which is extended down to low frequencies (Figure 4). The length differences of the steep slope which are associated with the capacitance of electrodes at low frequency region [34,35] may be due to the film thickness, correlated with the polymerization charge as shown in the inset of Figure 4. Although there is no semicircle in the high frequency region, slight deviations indicate fast charge transport from the polymer bulk as well as fast charge transfer to metal between polymer and solution interface.

Specific areal capacitance (C_{SP}) was calculated from CV curves of the polymer films in monomer-free solution based on earlier reports [36,37], the highest values were obtained at low scan rate (20 mVs^{-1}) coherently to pseudocapacitor theory [38].

As can be seen from Figure 4 and 5 insets, capacitances from CV and EIS have been correlated with polymer charge and scan rate of the polymerization which are proportional to the film thickness [39].

The electrochemical characteristics of the PProDOT-EtO-BZA films formed by CV can be clearly observed from the EIS results of the two very different substrates Pt and SPCE, respectively.

Moreover, the capacitance values, both C_{SP} and C_{LF} , of PProDOT-EtO-BZA coated on SPCE are at least two times higher than those of the polymer coated on the Pt electrode probably due to the nanostructured surface of SPCE [40,41].

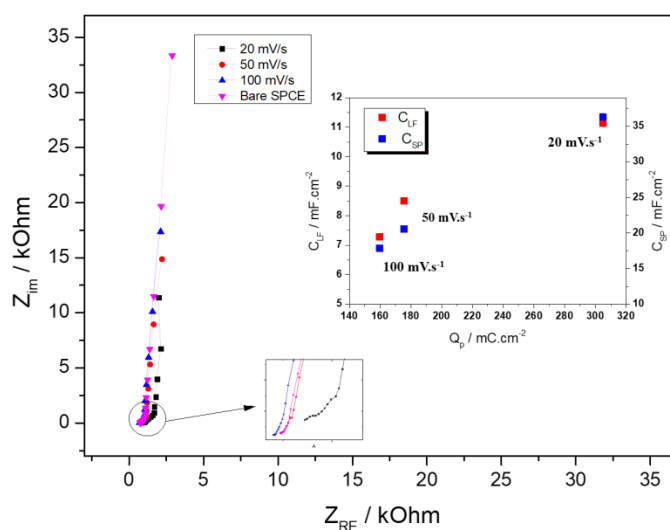


Figure 5. Nyquist plot of PProDOT-EtO-BZA coated at different scan rates on SPCE in the presence of $0.1\text{M Bu}_4\text{NPF}_6/\text{ACN}$, Insets: C_{LF} and C_{SP} (in monomer-free solution, for 20 mVs^{-1}) as a function of polymerization charge (Q_p) of coated films with different scan rates.

ProDOT-EtO-BZA **1** was electrochemically polymerized onto SPCE at 20 mVs^{-1} scan rate with 20 cycles for spectroscopic and morphological characterization of the PProDOT-EtO-BZA. Figure 6 shows the FTIR-ATR spectrum of the PProDOT-EtO-BZA film deposited from $\text{Bu}_4\text{NPF}_6/\text{ACN}$ electrolyte system. The band at 1514 cm^{-1} is assigned to the stretching vibration of the C=C bond of the thiophene ring. The bands at 1166 cm^{-1} and 1043 cm^{-1} arise from the C-O stretching vibration of the C-O-C unit of the alkylenedioxy group and of the ether side chain, respectively. Due to the presence of the PF_6^- ion in the polymer film the band at 832 cm^{-1} is corresponding to the P-F stretching vibration. Further vibrations from the C-S bond of the thiophene ring appear around 872 cm^{-1} [42]. The C=O stretching vibration of the carboxylic acid functional group occurs at $1682\text{--}1705 \text{ cm}^{-1}$. The broad signal in the region of $3000\text{--}2500 \text{ cm}^{-1}$ corresponds to the benzoic acid O-H stretching vibration.

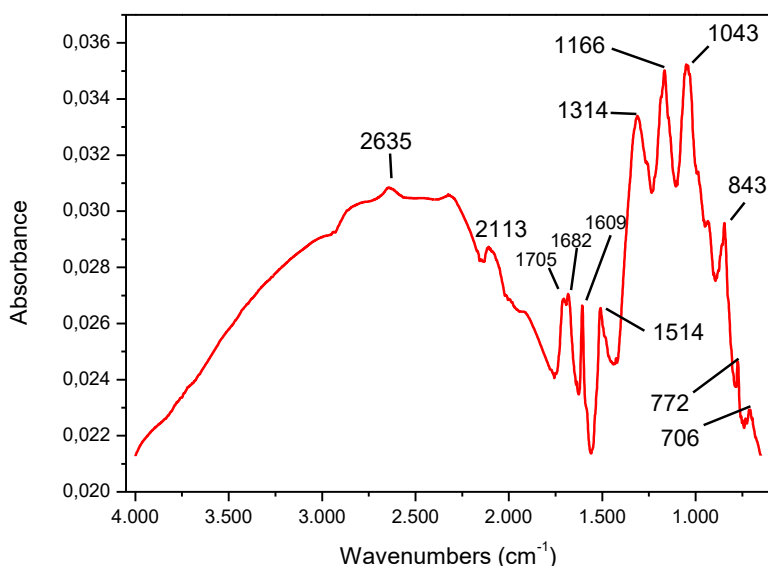


Figure 6. ATR-FTIR absorption bands and peak assignment of the PProDOT-EtO-BZA electro-deposited from $\text{Bu}_4\text{NPF}_6/\text{ACN}$.

SEM and AFM measurements were conducted in order to investigate the surface morphology and topography of the polymer film. Figure 7 shows the SEM images of bare and PProDOT-EtO-BZA coated SPCE. It is visible that the polymer film was distributed uniformly across the surface area of the electrode and images of higher magnification (inset) reveal clusters of densely packed nanofiber-like structures, similar to those of PProDOT derivatives functionalized by ethylenedioxy, alkoxy or thioalkyl side chains electrodeposited onto carbon fiber microelectrode [43], gold [44] and ITO glass [45], respectively. For bare SPCE a large grain structure had been observed [46].

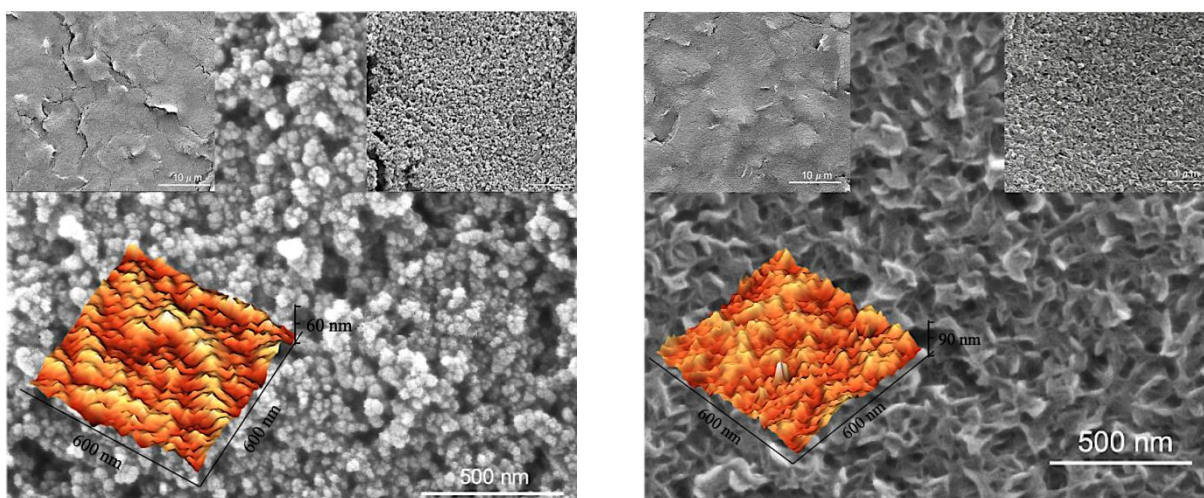


Figure 7. SEM images of bare SPCE (left) and PProDOT-EtO-BZA (right) film which was coated in the presence of 0.1M Bu₄NPF₆/ACN at 20 mVs⁻¹ on SPCE. Insets: magnified SEM images and 3D topographic images from AFM.

The root mean square (RMS) values describing the surface roughness of bare and coated SPCE (topographic images as insets of Figure 7) are given in Table 1. AFM measurements demonstrate that due to the microporous structure of the polymer film its surface roughness factor is approximately two times higher than that of bare SPCE. The RMS value of the unmodified SPCE [46] and the roughness factor increase observed for the polymer coated SPCE are comparable to earlier results obtained for PProDOT derivatives electrodeposited on different substrates [41].

Table 1. Surface roughness of bare PProDOT-EO-BZA coated SPCE

Sample	RMS Surface roughness (nm)
Bare SPCE	21.59
PProDOT-EtO-BZA	50.71

3.3. Comparative Study of the PProDOT derivatives on SPCE for Supercapacitor Application

PProDOT, PProDOT-EtO-BZA, PDBProDOT and PProDOT-Et₂ films were deposited onto SPCE from monomeric solution in 0.1 M Bu₄NPF₆/ACN via potentiodynamic electropolymerization at 50 mVs⁻¹ scan rate during 10 cycles (Figure 8). These conditions had been optimized for comparison of the different ProDOT derivatives.

The linear increase in current during polymer growth on the SPCE indicates electroactive film formation on the SPCE surface (Figure 8a-8d).

Similar to the results obtained for PProDOT-EtO-BZA, all PProDOT derivatives in this study showed linear relationship between current density (oxidation and reduction peaks of the polymer film) and square root of the scan rate, thus each polymer exhibits diffusional-controlled electrochemical processes on SPCE which is of critical importance for future applications of these materials.

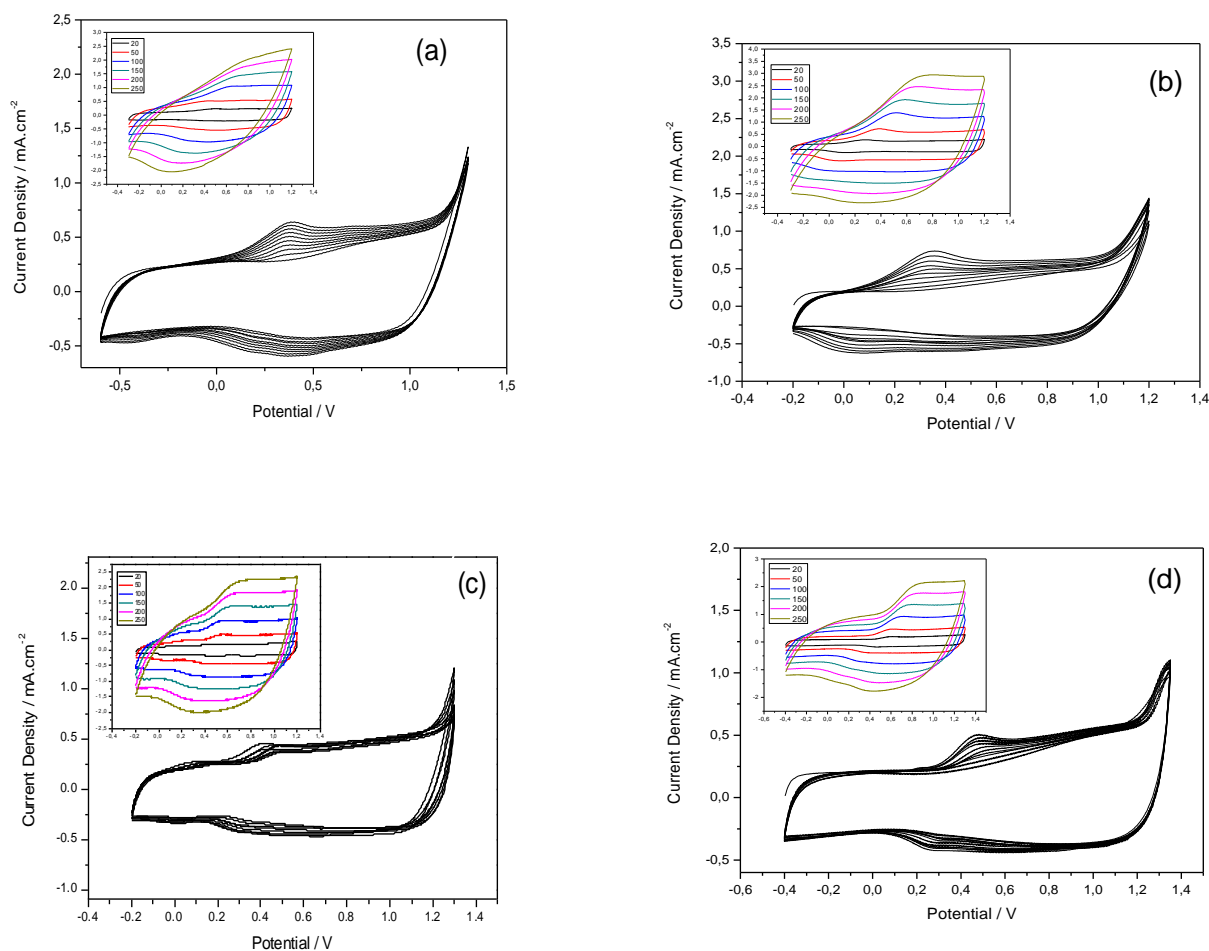


Figure 8. Potentiodynamic electropolymerization of a) ProDOT b) ProDOT-EtO-BZA c) ProDOT-Et₂ d) DBProDOT in 0.1 M Bu₄NPF₆/ACN on SPCE electrode at 50 mVs⁻¹. Insets: Monomer free measurement of polymer films with CV in 0.1 M Bu₄NPF₆/ACN at different scan rates between 20 and 250 mVs⁻¹

The oxidation onset potentials (E_{onset}) of the ProDOTs are shown in Table 2. The values in the range from 1.0 V to 1.3 V indicate the facile polymerizability of each monomer [47]. The value of DBProDOT (1.26 V) is higher than those of ProDOT (1.07 V), ProDOT-EtO-BZA **1** (1.06 V) and ProDOT-Et₂ (0.97 V), respectively which may be due to the rigid and bulky nature of the substituents [48] less stabilizing the radical cation intermediate and the electron withdrawing effect of the phenyl groups [41]. However, introduction of two electron donating alkyl groups into the ether bridge forming ProDOT-Et₂ [49] led to further decrease of the oxidation potential in comparison to ProDOT. The DBProDOT and ProDOT exhibit lower E_{onset} values on SPCE than on other substrates [41], revealing SPCE as an efficient substrate for electrochemical deposition of PProDOT derivatives.

Table 2. Values of E_{onset} of ProDOT monomers in 0.1 M $\text{Bu}_4\text{NPF}_6/\text{ACN}$.

	ProDOT	ProDOT-EtO-BZA	ProDOT-Et ₂	DBProDOT
$E_{\text{onset}}(\text{V})$	1.07	1.06	0.97	1.26

EIS measurements were conducted for investigation of the capacitive behavior in order to compare and correlate supercapacitor performance of PProDOT, PProDOT-EtO-BZA, PProDOT-Et₂ and PDBProDOT, respectively using SPCE as three electrode system in 0.1 M $\text{Bu}_4\text{NPF}_6/\text{ACN}$.

PProDOT and PProDOT-Et₂ were used for the fabrication of different types of supercapacitors [50-52,33] and PBPProDOT showed capacitive behavior on single carbon fiber microelectrode [24].

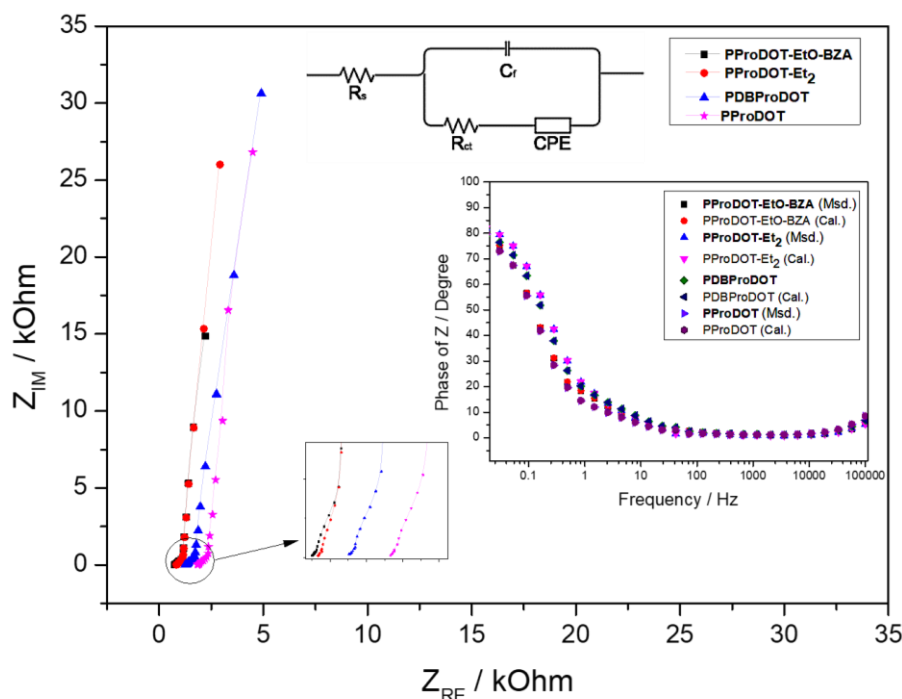


Figure 9. Nyquist plot of polymer films PProDOT, PProDOT-EtO-BZA, PProDOT-Et₂ and PDBProDOT in 0.1 M $\text{Bu}_4\text{NPF}_6/\text{ACN}$ on SPCE prepared under the same conditions Insets: Bode Phase plot (calculated and measured results) of PProDOT derivatives in 0.1 M $\text{Bu}_4\text{NPF}_6/\text{ACN}$ on SPCE prepared under the same conditions and ECM of PProDOT and its derivatives coated on SPCE.

Figure 9 illustrates Nyquist plots of films of PProDOT and PProDOT derivatives, respectively wherein the complex plane impedance curves displayed a nearly vertical straight line except for a slight knee in the low and high frequency region without semi-circle which refer to the properties of an ideal electrochemical capacitor and also low charge transfer resistance is consistent with ECM fitting results [53]. The insets of Figure 9 obtained from EIS measurements exhibit an ideal capacitive line (Bode phase angles close to 90°), indicating fast charge transfer at the interfaces of the SPCE to the polymer film and of the polymer film to the solution, respectively, as well as fast charge transport in the polymer bulk. The polymer films reach the maximum peak at 0.01 Hz with phase angles of 81.4°

for PDBProDOT, 83.6° for PProDOT-Et₂, 82.7° for PProDOT, and of 81.5° for PProDOT-EtO-BZA, respectively.

The ECM used for simulation is shown in the inset of Figure 9. In this simulation, experimental impedance data were used for the development of the circuit model $R(Q(R(C)))$ which was built up by the help of series components describing bulk solution and pore resistance of the polymer film and the electrolyte. Therein R_s means the polymer film capacitance and C_{LF} represents the charge transfer resistance at the interface between polymer film and electrolyte. R_{ct} , and CPE correspond to modelling of the double layer capacitance [41] associated with surface roughness [54]. The values of the circuit elements are given in Table 3 wherein n varies from 0 to 1. In general, a resistant reaching the value 0 or 1 exhibits pure capacitive behavior [55].

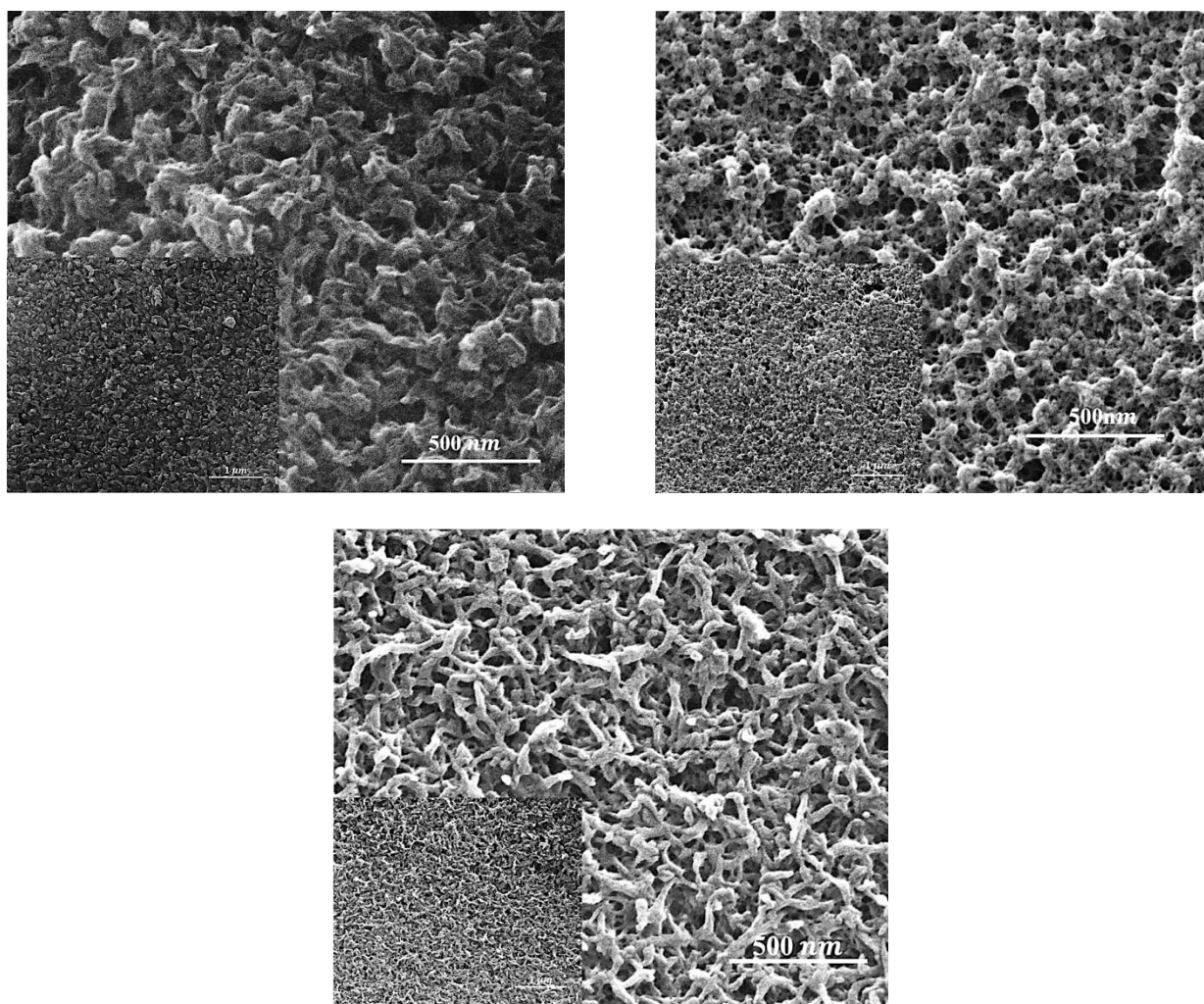


Figure 10. SEM images of PDBProDOT (left top), PProDOT-Et₂ (right top) and PProDOT (bottom) on SPCE.

The morphology of the PProDOT derivatives electrodeposited onto SPCE was investigated comparatively by SEM (Figure 10). The PProDOT-Et₂ film has a more ordered structure which is highly porous compared to PProDOT film due to the influence of the ethyl groups positioned above

and below the plane of the π -conjugated backbone suppressing π -stacking [56]. Agglomerated and separated structures were reported for DBPProDOT on ITO glass [41,57] owing to the rigid dibenzyl group which prevents interference of the polymer chains [48]. However packed nanofibers with small grain structure is seen more often on graphitic carbon like substrates (Figure 10, left top) [24]. It is also known that the polymerization charge has a significant effect on the aggregation [58]. Based upon the presence of intermolecular hydrogen bonding and “fusion” which is induced by increase of the length of the side chain, PProDOT-EtO-BZA showed a well packed fiber structure compared to PProDOT [59].

Table 3. Data calculated from ECM for PProDOTs of this study compared to PProDOT-EtO-BZA

	PProDOT	PProDOT-EtO-BZA	PProDOT-Et ₂	DBPProDOT
R _s (ohm.cm ²)	15.8	96.51	106	134.1
C _f (mF.cm ⁻²)	0.76	1.23	0.94	0.96
CPE (S.s ⁻ⁿ .cm ⁻²)	2.65E-3	6.04E-3	3.4E-3	3.1E-3
Freq. Power (n)	0.85	0.94	0.95	0.93
R _{ct} (ohm.cm ²)	77.24	54.88	57.86	71.44
Chi squared (x ²)	3.65E-3	2.05E-3	1.4E-3	2.26E-3

Figure 11 represents calculated and cited [24,33,41] capacitance values of the ProDOT derivatives considered wherein C_{LF}, low frequency capacitance was obtained from EIS (eq. 1), C_{SP}, areal specific capacitance was determined from monomer free CV curves, C_f, film capacitance was estimated from ECM fitted values, and C_{PSC}, pseudo-capacitance was deduced from ECM fitted values which were calculated by ZSimpWin (3.30) with theory of CPE [60].

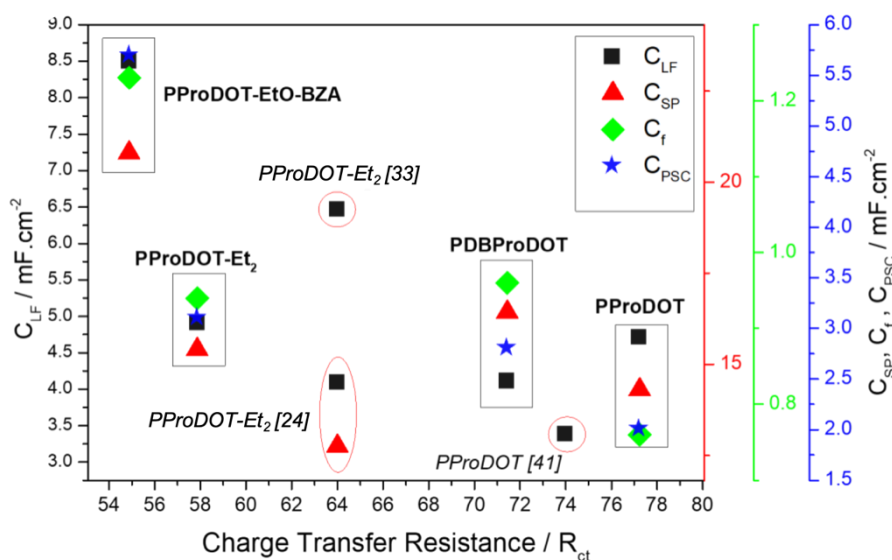


Figure 11. Variation of calculated and cited C_{LF}, C_{SP}, C_f, C_{PSC} (pseudo-capacitance) of the PProDOT derivatives on SPCE.

Apart from the present work the investigation of the capacitive behavior of several PProDOTs bearing molecular units approximating the chemical structure of PProDOT-EtO-BZA and their application in supercapacitor devices is described in the literature (Table 4).

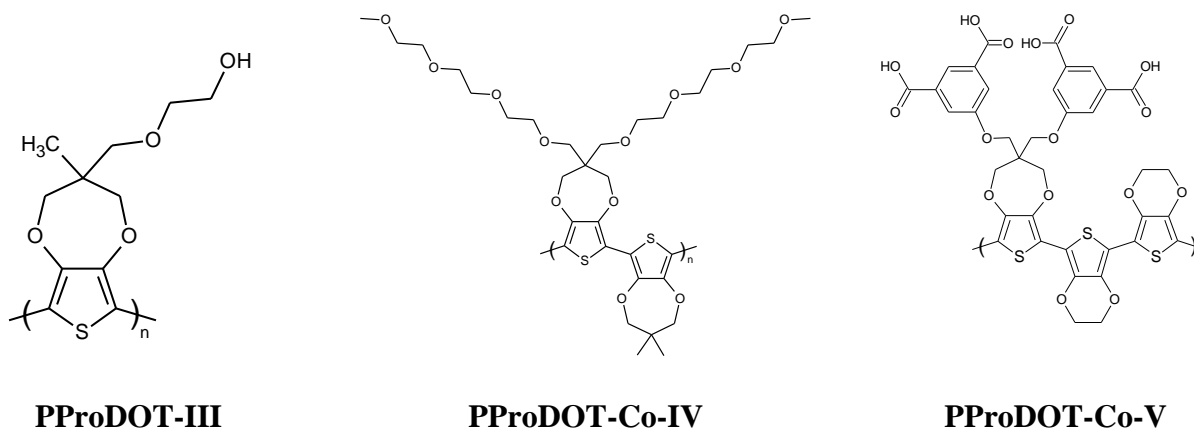
Table 4. Capacitance values of PProDOTs structurally approximating PProDOT-EtO-BZA

PProDOT-Me ₂	PProDOT-Bu ₂	PProDOT-III	PProDOT-Co-IV	PProDOT-Co-V
C = 55 F/g q = 25 mC/cm ² [61]	C _{dl} = 62 mF/cm ² [64]	C _{LF} = 34.6 mF/cm ² [43]	C > 80 F/g [66]	C = 54 F/g [67]
q = 18.5 mC/cm ² [62]				
C _{LF} = 12.05mF/cm ² [63]				

The 2',2'-dimethyl PProDOT derivative is a far-off approach to the structure of PProDOT-EtO-BZA since oligoether or carboxy-functionalized molecular units are missing. PProDOT-Me₂ coated onto gold/Kapton via potentiodynamic deposition from 0.1M LiBTI/ACN exhibited a specific capacitance of C = 55 F/g wherein during five deposition scans a charge of q = 25 mC/cm² was exchanged. During the electrodeposition of PProDOT-Me₂ onto single carbon fiber microelectrode (SCFME) from 0.1M Bu₄NPF₆/ACN using the same method an exchange of charge of q = 18.5 mC/cm² was measured [62] and a low frequency capacitance value of 12.05 mF/cm² was calculated [63]. As a consequence of its capacitive properties PProDOT-Me₂ was used for the fabrication of Type I supercapacitors [61].

In spite of the non-polar character of its substituents at the ether bridge the 2',2'-dibutyl PProDOT derivative is mimicking the steric hindrance of the functionalized side chain of PProDOT-EtO-BZA. For PProDOT-Bu₂ electrodeposited onto SCFME from 0.1M NaClO₄/ACN a double layer capacitance value of C_{dl} = 62 mF/cm² was determined [64].

The hydroxyether-functionalized PProDOT-III bearing a part of an oligoether unit as side chain depicts a closer approach to the molecular structure of PProDOT-EtO-BZA. For the PProDOT-III electro-polymerized on SCFME from 0.1M Et₄NPF₆/ACN a low frequency capacitance value of C_{LF} = 34.6 mF/cm² was calculated from EIS measurements [43].



Recently, solution processable PProDOT copolymers bearing alkoxy groups have been developed for supercapacitor application and the capacitive behavior was evaluated for polymer films prepared by drop casting on glassy carbon electrodes [65].

PProDOT-Co-IV bearing dioxyethylene units at a chain length similar to PProDOT-EtO-BZA was synthesized by palladium-catalyzed copolymerization of the oligoether functionalized ProDOT and 2,5-dibromo-ProDOT-Me₂. The gravimetric capacitance of PProDOT-Co-IV was calculated from CVs recorded on glassy carbon in NaCl/H₂O and Bu₄NPF₆/PC, respectively to be $C > 80$ F/g [66].

PProDOT-Co-V carrying aromatic carboxylic groups as one element of the molecular structure of PProDOT-EtO-BZA can be processed from aqueous solution via carboxylate exhibiting a gravimetric capacitance of $C = 54$ F/g after restoring the carboxylic functional group. PProDOT-Co-V was coated onto nonwoven carbon nanotube textile and applied to the fabrication of symmetrical, flexible super-capacitors [67].

Since ProDOT-EtO-BZA **1** combines structural units of solution processable PProDOT copolymers it will be possible to design new copolymers from **1**, which can be dissolved in organic solvents, by copolymerizing **1** in the presence of a ProDOT derivative functionalized appropriately.

For the development of water processable copolymers from **1** the carboxylic functional group in **1** has to be protected as an ester in advance of the copolymerization in order to prepare the carboxylate [25] by alkaline saponification of the ester.

4. CONCLUSION

ProDOT-EtO-BZA **1** was electropolymerized on SPCE and Pt wire, respectively, via CV and the electrochemical and morphological properties of the corresponding PProDOT-EtO-BZA were explored. The results show that the chemical structure of **1** has a crucial effect on the electrochemistry and in particular, the capacitive behavior of the polymer film. ProDOT, DBProDOT and ProDOT-Et₂ and ProDOT-EtO-BZA were also homogeneously coated on SPCE via CV. It was observed that the oxidation potential of ProDOT-EtO-BZA is quite similar to that of ProDOT indicating the suitability of the polymer for various applications. It is evidenced that the structure of **1** has a significant effect on the capacitive behavior of the PProDOT-EtO-BZA. Moreover, comparison of given and cited results indicated that the capacitance values (C_{LF} , C_{SP} , C_f , C_{PSC}) of PProDOT-EtO-BZA (8.5 mF/cm², 20.8 mF/cm², 1.23 mF/cm² and 5.7 mF/cm², respectively) are approximately two times higher than those of the other PProDOT derivatives investigated in this study. In addition, correlation between calculated R_{ct} and different capacitance values obtained by electrochemical methods was observed as well as the coherence of the data. Due to the molecular structure of **1** new PProDOT copolymers processable from organic solvents and water can be designed. These results demonstrate that ProDOT-EtO-BZA **1** is a powerful candidate for supercapacitor application.

References

1. T. Chen, Q. Chen, G. Liu and G. Chen, *J. Appl. Polym. Sci.*, 135 (2018) 45943.

2. T. Y. Kim, W. Wei, T. K. Lee, B. S. Kim, S. C. Park, S. Lee, E. H. Suh, J. Jang, J. Bisquert and Y. S. Kang, *ACS Appl. Mater. Interfaces*, 10 (2018) 2537.
3. B. Çelik, I. Çelik, H. Dolaş, H. Görçay, Y. Şahin, A. S. Sarac and K. Pekmez, *React. Funct. Polym.*, 83 (2014) 107.
4. Y. Han and L. Dai, *Macromol. Chem. Phys.*, 220 (2019) 1800355.
5. R. Balint, N. J. Cassidy and S. H. Cartmell, *Acta Biomater.*, 10 (2014) 2341.
6. K. K. Tintula, S. Pitchumani, P. Sridhar and A. K. Shukla, *J. Chem. Sci.*, 122 (2010) 381.
7. N. He, S. Papp, T. Lindfors, L. Höfler, R. M. Latonen and R. E. Gyurcsányi, *Anal. Chem.*, 89 (2017) 2598.
8. N. Aydemir, J. Malmström and J. Travas-Sejdic, *Phys. Chem. Chem. Phys.*, 18 (2016) 8264.
9. K. D. Fong, T. Wang and S. K. Smoukov, *Sustain. Energy Fuels*, 1 (2017) 1857.
10. P. Simon and Y. Gogotsi, *Acc. Chem. Res.*, 46 (2013) 1094.
11. A. J. Illott, N. M. Trease, C. P. Grey and A. Jerschow, *Nat. Commun.*, 5 (2014) 4536.
12. P. J. Hall, M. Mirzaeian, S. I. Fletcher, F. B. Sillars, A. J. R. Rennie, G. O. Shitta-Bey, G. Wilson, A. Cruden and R. Carter, *Energy Environ. Sci.*, 3 (2010) 1238.
13. Y. Zhang, Z. Wei, H. Li, L. Cai and J. Pan, *IEEE Trans. Smart Grid*, 10 (2019) 227.
14. N. Ghaviha, J. Campillo, M. Bohlin and E. Dahlquist, *Energy Procedia*, 105 (2017) 4561.
15. Q. Meng, K. Cai, Y. Chen and L. Chen, *Nano Energy*, 36 (2017) 268.
16. G. A. Snook, P. Kao and A. S. Best, *J. Power Sources*, 196 (2011) 1.
17. M. Ates and A. S. Sarac, *Polym.-Plast. Technol. Eng.*, 50 (2011) 1130.
18. A. Laforgue, P. Simon, J. F. Fauvarque, M. Mastragostino, F. Soavi, J. F. Sarrau, P. Lailier, M. Conte, E. Rossi and S. Saguatti, *J. Electrochem. Soc.*, 150 (2003) A645.
19. A. Laforgue, P. Simon, C. Sarrazin and J.-F. Fauvarque, *J. Power Sources*, 80 (1999) 142.
20. A. Di Fabio, A. Giorgi, M. Mastragostino and F. Soavi, *J. Electrochem. Soc.*, 148 (2001) A845.
21. C. Arbizzani, M. C. Gallazzi, M. Mastragostino, M. Rossi and F. Soavi, *Electrochem. Commun.*, 3 (2001) 16.
22. G. G. Rodríguez-Calero, M. A. Lowe, Y. Kiya and H. D. Abruña, *J. Phys. Chem., C* 114 (2010) 16776.
23. J. Roncali, *Macromol. Rapid Commun.*, 28 (2007) 1761.
24. A. S. Sarac, S. E. Ozgul, A. Gencturk, B. Schulz, H.-D. Gilsing and H. Faltz, *Prog. Org. Coat.*, 69 (2010) 527.
25. K. J. Jetzschmann, G. Jágerszki, D. Dechtrirat, A. Yarman, N. Gajovic-Eichelmann, H.-D. Gilsing, B. Schulz, R. E. Gyurcsányi and F. W. Scheller, *Adv. Funct. Mater.*, 25 (2015) 5178.
26. P. Fanjul-Bolado, P. Queipo, P. J. Lamas-Ardisana and A. Costa-García, *Talanta*, 74 (2007) 427.
27. J. Liu, J. Wang, C. Xu, H. Jiang, C. Li, L. Zhang, J. Lin and Z. X. Shen, *Adv. Sci.*, 5 (2018) 1700322.
28. C. C. Hu and T. W. Tsou, *Electrochim. Acta*, 47 (2002) 3523.
29. H. Wang, Q. Hao, X. Yang, L. Lu and X. Wang, *Nanoscale*, 2 (2010) 2164.
30. B. Akinwolemiwa, C. Peng and G. Z. Chen, *J. Electrochem. Soc.*, 162 (2015) A5054.
31. T. Karazehir, M. Ates and A. S. Sarac, *Int. J. Electrochem. Sci.*, 10 (2015) 6146.
32. M. Tokita, M. Egashira, N. Yoshimoto and M. Morita, *Electrochemistry*, 80 (2012) 752.
33. C. Y. Hsu, H. W. Chen, K. M. Lee, C. W. Hu and K. C. Ho, *J. Power Sources*, 195 (2010) 6232.
34. R. Farma, M. Deraman, Awitdrus, I. A. Talib, R. Omar, J. G. Manjunatha, M. M. Ishak, N. H. Basri and B. N. M. Dolah, *Int. J. Electrochem. Sci.*, 8 (2013) 257.
35. M. Hughes, M. S. P. Shaffer, A. C. Renouf, C. Singh, G. Z. Chen, D. J. Fray and A. H. Windle, *Adv. Mater.*, 14 (2002) 382.
36. X. Sun, G. Wang, J. Y. Hwang and J. Lian, *J. Mater. Chem.*, 21 (2011) 16581.
37. T. Zhai, F. Wang, M. Yu, S. Xie, C. Liang, C. Li, F. Xiao, R. Tang, Q. Wu, X. Lu and Y. Tong, *Nanoscale*, 5 (2013) 6790.
38. Y. Zhao, Z. Wang, R. Yuan, Y. Lin, J. Yan, J. Zhang, Z. Lu, D. Luo, J. Pietrasik, M. R. Bockstaller

- and K. Matyjaszewski, *Polymer*, 137 (2018) 370.
39. J. Bobacka, A. Lewenstam, A. Ivaska and A. Fin, *J. Electroanal. Chem.*, 489 (2000) 17.
 40. A. S. Sarac, M. Ates and B. Kilic, *Int. J. Electrochem. Sci.*, 3 (2008) 777.
 41. Y. Sulaiman and R. Katakay, *J. Electrochem. Soc.*, 159 (2012) F1.
 42. F. G. Guler and A. S. Sarac, *Express Polym. Lett.*, 5 (2011) 493.
 43. F. G. Guler, H.-D. Gilsing, B. Schulz and A. S. Sarac, *J. Nanosci. Nanotechnol.*, 12 (2012) 7869.
 44. M. Lamy, T. Darmanin and F. Guittard, *Colloid Polym. Sci.*, 293 (2015) 933.
 45. B. Wei, L. Ouyang, J. Liu and D. C. Martin, *J. Mater. Chem. B*, 3 (2015) 5028.
 46. T. S. C. R. Rebelo, C. M. Pereira, M. G. F. Sales, J. P. Noronha, J. Costa-Rodrigues, F. Silva and M. H. Fernandes, *Anal. Chim. Acta*, 850 (2014) 26.
 47. J. Niu, S. Chen, W. Zhang, W. Zhang, K. Chai, G. Ye, D. Li, W. Zhou, X. Duan and J. Xu, *Electrochim. Acta*, 283 (2018) 488.
 48. K. Krishnamoorthy, A. V. Ambade, M. Kanungo, A. Q. Contractor and A. Kumar, *J. Mater. Chem.*, 11 (2001) 2909.
 49. C. L. Gaupp, D. M. Welsh and J. R. Reynolds, *Macromol. Rapid Commun.*, 23 (2002) 885.
 50. J. D. Stenger-Smith, C. K. Webber, N. Anderson, A. P. Chafin, K. Zong and J. R. Reynolds, *J. Electrochem. Soc.*, 149 (2002) A973.
 51. J. D. Stenger-Smith, A. Guenther, J. Cash, J. A. Irvin and D. J. Irvin, *J. Electrochem. Soc.* 157 (2010) A298.
 52. L. Xiang, A. Ali, R. Jamal, S. Ding, Z. Zhong and T. Abdiryim, *Polym. Compos.*, 40 (2019) 1989.
 53. C. Xu, F. Xu, L. Sun, L. Cao, F. Yu, H. Zhang and E. Yan, *Int. J. Electrochem. Sci.*, 14 (2019) 1782.
 54. D. S. Vieira, P. R. G. Fernandes, H. Mukai, R. S. Zola, G. G. Lenzi and E. K. Lenzi, *Int. J. Electrochem. Sci.*, 11 (2016) 7775.
 55. N. H. Basri, M. Deraman, M. Suleman, N. S. M. Nor, B. N. M. Dolah, M. I. Sahri and S. A. Shamsudin, *Int. J. Electrochem. Sci.*, 11 (2016) 95.
 56. J. H. Huang, Z. Y. Ho, D. Kekuda, C. W. Chu and K. C. Ho, *J. Phys. Chem. C*, 112 (2008) 19125.
 57. R. Lakshmanan, P. P. Raja, N. C. Shivaprakash and S. S. Nair, *J. Appl. Polym. Sci.*, 131 (2014) 40717.
 58. K. M. Lee, P. Y. Chen, C. Y. Hsu, J. H. Huang, W. H. Ho, H. C. Chen and K. C. Ho, *J. Power Sources*, 188 (2009) 313.
 59. T. Darmanin and F. Guittard, *Mater. Chem. Phys.*, 146 (2014) 6.
 60. J. J. Santana Rodríguez, F. J. Santana Hernández and J. E. González González, *Mater. Corros.*, 57 (2006) 778.
 61. D. Y. Liu and J. R. Reynolds, *ACS Appl. Mater. Interfaces*, 2 (2010) 3586.
 62. A. S. Sarac, H.-D. Gilsing, A. Gencturk and B. Schulz, *Prog. Org. Coat.*, 60 (2007) 281.
 63. A. S. Sarac and A. Gencturk, *Low-Dimensional and Nanostructured Materials and Devices*, H. Ünlü, N. J. M. Horing and J. Dabowski, (Eds.), Springer, New York (2016), p. 461.
 64. M. C. Turhan, A. S. Sarac, A. Gencturk, H.-D. Gilsing, H. Faltz and B. Schulz, *Synth. Met.*, 162 (2012) 511.
 65. A. M. Österholm, J. F. Ponder, J. A. Kerszulis and J. R. Reynolds, *ACS Appl. Mater. Interfaces*, 8 (2016) 13492.
 66. L. R. Savagian, A. M. Österholm, J. F. Ponder, K. J. Barth, J. Rivnay and J. R. Reynolds, *Adv. Mater.*, 30 (2018) 1804647.
 67. A. W. Lang, J. F. Ponder, A. M. Österholm, N. J. Kennard, R. H. Bulloch and J. R. Reynolds, *J. Mater. Chem. A*, 5 (2017) 23887.